Maximal Force Characteristics of the Ca^{2+}-Powered Actuator of *Vorticella convallaria*

Sangjin Ryu,[†¶] Matthew J. Lang,[†§] and Paul Matsudaira[‡§¶*]
[†]Department of Mechanical Engineering, [‡]Department of Biology, and [§]Department of Biological Engineering, Massachusetts Institute of Technology, Cambridge, Massachusetts; and [¶]Whitehead Institute for Biomedical Research, Cambridge, Massachusetts

ABSTRACT The millisecond stalk contraction of the sessile ciliate *Vorticella convallaria* is powered by energy from Ca^{2+} binding to generate contractile forces of ~10 nN. Its contractile organelle, the spasmoneme, generates higher contractile force under increased stall resistances. By applying viscous drag force to contracting *V. convallaria* in a microfluidic channel, we observed that the mechanical force and work of the spasmoneme depended on the stalk length, i.e., the maximum tension (150–350 nN) and work linearly depended on the stalk length (~2.5 nN and ~30 fJ per 1 μm of the stalk). This stalk-length dependency suggests that motor units of the spasmoneme may be organized in such a way that the mechanical force and work of each unit cumulate in series along the spasmoneme.

INTRODUCTION

The sessile ciliated protozoan *Vorticella convallaria* is capable of retracting its ~50-μm-long cell body or zooid through a distance of ~100 μm in <10 ms by contracting its inner-stalk contractile fiber, the spasmoneme (Fig. 1 *A* and Fig. S1 in the Supporting Material) (1). At its peak during normal contraction in water, it can reach speeds of ~60 mm/s and contraction forces of ~30 nN (2). The mechanical work and peak power output of this process are ~2 pJ and ~2 nW, respectively. This rapid stalk coiling, which presumably is done for threat evasion or mixing enhancement, characterizes *V. convallaria* as the fastest animal in terms of length-specific velocity (*V. convallaria:* ~1200; fruit fly: ~950; cheetah: ~24; and yellowfin tuna: ~21; unit: body length/s) (3,4). However, the mechanical mechanism of the spasmoneme contraction is unknown.

Experiments on permeabilized stalks have shown that the stalk contraction is powered by binding of calcium ions (11.2 kJ/mol) and not hydrolysis of ATP (30.5 kJ/mol) (5,6). The major Ca^{2+}-binding protein of the spasmoneme is spasmin, a 20 kDa EF-hand Ca^{2+}-binding protein (7,8). The spasmoneme consists of filaments (2–4 nm in diameter) and membranous tubules for intracellular Ca^{2+} storage (9). It is speculated that the filaments contain spasmin, and thus they either coil or shorten upon Ca^{2+} binding (10,11). Because the filaments are oriented longitudinally in the spasmoneme, their molecular-scale shortening is suggested to cause shortening of the spasmoneme at the organelle scale and coiling of the stalk at the cell scale (9,12). Because of its unique contraction features, the spasmoneme of *V. convallaria* is regarded as a model system of Ca^{2+}-based cell motility and biomimetic smart materials (13).

The maximum contraction force and energetics of the spasmoneme not only mechanistically characterize the stalk contraction of *V. convallaria* (14) but also set physical bounds for any possible contraction mechanism models. Therefore, we aimed to measure the isometric tension of the spasmoneme (the maximum tension developed without a change in the stalk length) and its mechanical work under an external resistance. Because of the small size and millisecond contractions of live *V. convallaria*, its force was evaluated based on fluid dynamic modeling (2,6,15) or measured from permeabilized *V. convallaria* (average isometric tension $\approx$ 40 nN) (16). Larger ciliates with a spasmoneme were also tested for tension measurements (isometric tension of permeabilized *Zoothamnium*: ~28 μN (17); contractile tension of live *Carchesium*: 4–8 μN (18)). In the case of live *V. convallaria*, a load can be externally applied to hinder the stalk contraction for isometric force measurements and energetics analyses. As an external stall resistance rises, the stalk contracts more slowly with increased final end-to-end length, and the coiled stalk retains a higher residual contraction force (2,15,19). Therefore, it is possible to estimate the isometric tension of live *V. convallaria* by extrapolating the residual contraction force against the stalk length ratio (= contracted stalk length/extended stalk length) (19). Recent applications of centrifugal force and the elastic restoring force of a micropipette to contracting *V. convallaria* suggested that the spasmoneme can generate a contractile force of up to a few hundred nanonewtons (19). However, these experiments did not control the magnitude of the stall force in situ or measure the isometric tension of individual *V. convallaria* cells.

Submitted February 7, 2012, and accepted for publication July 23, 2012.

*Correspondence: dbsmpt@nus.edu.sg

Sangjin Ryu's present address is Department of Mechanical and Materials Engineering, University of Nebraska-Lincoln, Lincoln, NE.

Matthew J. Lang's present address is Department of Chemical and Biomolecular Engineering, and Department of Molecular Physiology and Biophysics, Vanderbilt University, Nashville, TN.

Paul Matsudaira's present address is Department of Biological Science, National University of Singapore, Singapore.

Editor: Shin'ichi Ishiwata.

0006-3495/12/09/0860/8 $2.00

http://dx.doi.org/10.1016/j.bpj.2012.07.038

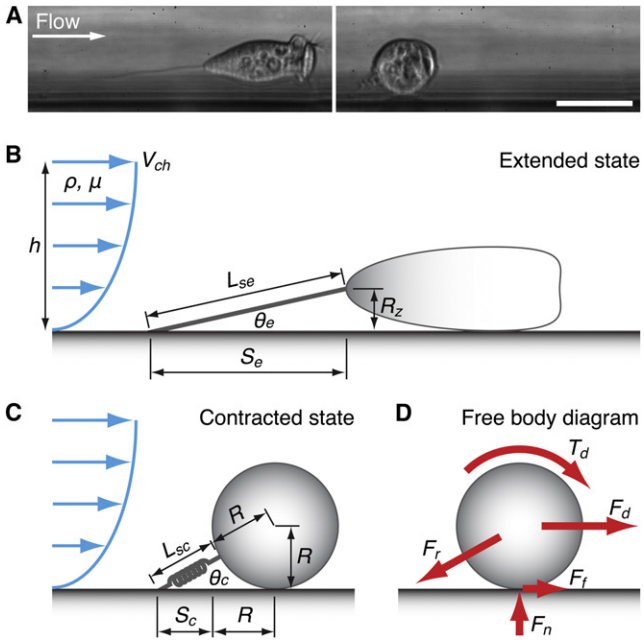

FIGURE 1 *V. convallaria* in the microfluidic channel. (*A*) Side view of relaxed (*left*) and contracted (*right*) *V. convallaria* (6.9 cP, 1 ml/min) in the PDMS channel. The relaxed zooid was roughly parallel to the channel surface, and the contracted zooid was in contact with the surface. Scale bar: 50 μm. (*B* and *C*) Simplified models for relaxed and contracted *V. convallaria* in Poiseuille flow (ρ, fluid density; θ, angle between the stalk and channel surface). Flow conditions were chosen to satisfy the following creeping-flow condition: $2\rho R^2 V_{ch}/\mu h < 0.2$ (see Supporting Material) (46). (*D*) Free body diagram for forces acting on the contracted zooid. F_n : normal force ($= F_r \sin\theta_c$), F_f : friction force ($= T_d/R$). See the text for the rest of the symbols.

To circumvent these technical problems in measuring the isometric force, we applied a viscous drag force to live *V. convallaria* adherent to the surface of a microfluidic channel by flowing polyvinylpyrrolidone (PVP) solutions (viscosity: 1.0, 2.7, 6.9, and 10.3 cP) at various flow rates (1, 5, 10, and 15 ml/min) against the direction of contraction (Fig. 1 *A*). A microfluidic platform has several advantages compared with previous approaches. First, it allows one to control the stall force by changing the medium viscosity and flow rate. Second, the platform enables one to change the chemical environment of *V. convallaria* by introducing various reagents into the channel. Lastly, it is possible to observe multiple stalk contraction cycles of single cells under different stall conditions. In the channel flow, the drag force on the zooid stalled the stalk contraction, and the spasmoneme generated higher contractile force with the increasing resistance. Furthermore, the isometric tension and mechanical work of the spasmoneme showed a dependence on the stalk length. Based on this stalk-length dependence, we suggest that the spasmoneme may have a structure in which the mechanical force and work of each motor unit accumulate in parallel across the cross section and in series along the length of the spasmoneme. This hypothesis enabled estimations of maximum force and work per motor unit.

MATERIALS AND METHODS

Cell culture and channel injection

V. convallaria cells were cultured in the laboratory (20) as described elsewhere (2). In brief, the cells were grown in flasks with wheat fusion solution. Solution from two flasks was poured into a sterile flask after being shaken, and the cells were allowed to grow their stalk overnight. After a change of medium and another shaking, the cells were filtered with micromesh (50-μm Nitex nylon mesh; Sefar Filtration, Depew, NY). The filter was laid on a petri dish filled with spring water (Poland Spring, Poland, ME) so that the cells could pass through the filter and attach onto the bottom. Cells on the dish bottom were scraped and transferred to a microcentrifuge container. The cells were centrifuged at 2900 $\times$ *g* for 10 min and resuspended in fresh spring water, and then harvested cells were injected into 5 $\times$ 50 $\times$ 0.4 mm^3 microfluidic channels (μ-Slide I; Ibidi, Martinsried, Germany). The cells were allowed 1–2 days to attach to the channel surface and grow their stalk.

Side-view channel fabrication

In addition to the plastic channel that accommodated only top-view observation, a channel for side-view observation was fabricated with polydimethylsiloxane (PDMS; Sylgard 184 Silicone Elastomer Kit; Dow Corning, Midland, MI). The side-view channel had the same cross-sectional dimension as the top-view channel, but one of its short sides faced the bottom. Because of the high aspect ratio of the PDMS channel, a channel mold was machined from aluminum alloy. In the PDMS channel, cells on a sidewall were observed with an objective lens with a long working distance, which was required to develop the hydrodynamic model of *V. convallaria* in the channel (Fig. 1 *A*).

Hydrodynamic model for residual contraction force estimation

Our approach required a model to estimate the cell dimensions from top-view images (Fig. 2 *A*) and then extract the residual contraction force from viscous drag on the zooid. In the extended state (Fig. 1 *B*), the zooid was assumed to be a body of revolution parallel to the flow direction touching the surface. The stalk length L_{se} was determined from the projected length of the stalk S_e and the zooid width R_z : $L_{se} = R_z/\sin\theta_e$ where $\theta_e = \tan^{-1}(R_z/S_e)$. In the contracted state (Fig. 1 *C*), the zooid was modeled as a sphere touching the surface with its center on the extension of the stalk, and the final stalk length L_{sc} was estimated from the projected stalk length S_c and the zooid radius R: $L_{sc} = R/\sin\theta_c - R$ where $\theta_c = \tan^{-1}[R/(S_c + R)]$. Here, subscripts e and c stand for extended and contracted states, respectively.

Because *V. convallaria* was located in creeping Poiseuille flow with a one-dimensional parabolic velocity profile, the contracted zooid experienced not only a drag force $F_d = 6\pi\mu R V_{ch} F^p$ but also torque $T_d = 8\pi\mu R^2 V_{ch} T^p$ (Fig. 1 *D*), where μ is the fluid viscosity and V_{ch} is the flow speed at the channel center. F^p and T^p are the correction factors to take into account the wall effect of the channel surface on viscous drag force and torque, respectively ($F^p = R/3h[10.2 - 5.82(R/h)]$, $T^p = R/4h[3.78 - 3.96(R/h)]$), and $2h$ is the channel height (see Supporting Material) (21). According to the torque balance at the zooid-surface contact point, the residual contraction force of the stalk F_r was obtained with $F_r = (F_d + T_d/R)/\cos\theta_c$.

CFD simulations of the channel flow

The residual contraction force estimation model required cells to be located in one-dimensional Poiseuille flow. Therefore, it was necessary to identify the experiment zone in the channel where the flow was one-dimensional.

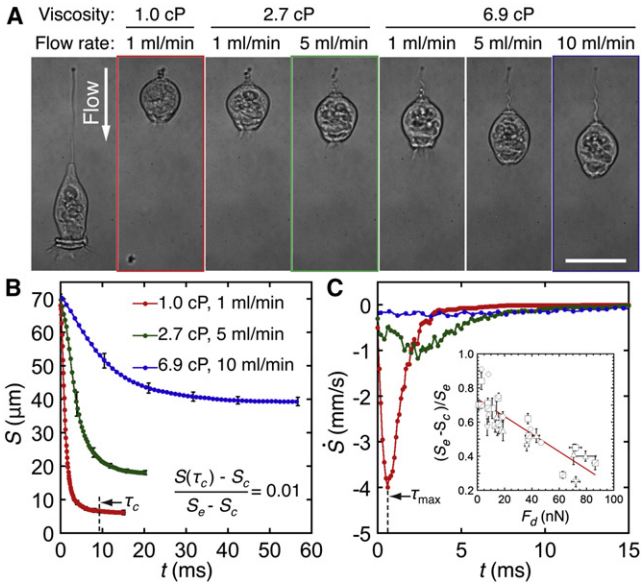

FIGURE 2 Stalled stalk contraction of *V. convallaria*. (*A*) Stalled contraction of *V. convallaria* (top view). The leftmost picture shows the extended state, and the rest show contracted states under different flow conditions. The stalk contraction was stalled more as the fluid viscosity and/or flow rate increased. Scale bar: 50 μm. (*B*) Averaged projected stalk length S of three representative stalled contractions ($n = 4$–5 contractions). (*C*) Averaged approximated contraction rate $\dot{S}$ ($= dS/dt$). Inset: Approximated stalk-length change ratios $(S_e - S_c)/S_e$ versus the zooid drag force F_d. The red fitting line suggests $(S_e - S_c)/S_e \sim F_d^{-1}$. Error bars: standard deviation (SD).

For this purpose, the channel flow was simulated using COMSOL Multiphysics (COMSOL, Burlington, MA; see Supporting Material).

Experimental setup

One end of the channel was connected to a 60 ml syringe installed on a syringe pump (PHD22/2000; Harvard Apparatus, Holliston, MA) and the other end was led to a waste dump. In addition to spring water, PVP solutions of 1%, 2%, and 3% w/w concentration (pH 6.5–7.0; MW 360,000; Sigma-Aldrich, St. Louis, MO) were injected into the channel at various flow rates (1, 5, 10, and 15 ml/min). The PVP solution properties were measured as described elsewhere (2), and the measured viscosities were 1.0, 2.7, 6.9, and 10.3 cP, respectively (see Table S2 for fluid properties).

For image acquisition, we used two high-speed cameras: Phantom V7 (Vision Research, Wayne, NJ) for high temporal resolution (10,000 fps) and FASTCAM-PCI (Photron, San Diego, CA) for low temporal resolution (30 fps). An inverted light microscope (Eclipse TE300; Nikon Instruments, Melville, NY) was used with a 40× objective lens (NA 0.6, 0.5 μm/pixel) for high-frame-rate imaging, and a 20× objective lens (NA 0.45, 0.79 μm/pixel) was used for low-frame-rate imaging. The size of the acquired images was 512 × 256 pixels. MATLAB (The MathWorks, Natick, MA) was used to postprocess the images and to measure the dimensions of cells.

Once an appropriate cell was chosen, four to five contractions of the cell were recorded for each flow condition. Between recordings, the cell was allowed to rest for a few minutes. When the medium needed to be changed, the injection rate was set to low (0.2–0.5 ml/min) to avoid fatiguing the cell, and the cell was allowed to rest for 10–30 min. Viscous media of low to high viscosities were injected. Depending on the cell's status, stall conditions were determined. In some cases, we applied a low flow rate and/or low PVP concentration in the middle of a high stall force condition to examine whether the stalk could contract normally. If the cell showed abnormal contractions, the corresponding data set was discarded.

RESULTS

Stalled contraction and isometric tension measurement

We investigated how the viscous resistance stalled the stalk contraction of *V. convallaria* based on the projected stalk length S. As the flow rate and/or the medium viscosity increased, leading to a higher stall force, *V. convallaria* contracted over a shorter distance and took a longer time. That is, the projected length of the contracted stalk S_c and contraction time τ_c increased with the applied resistance (Figs. 2 *B* and 3 *A*). Here τ_c was defined as time when $(S - S_c)/(S_e - S_c) = 0.01$. As a result, the contraction distance ratio $(S_e - S_c)/S_e$, the mean contraction rate $|\bar{\dot{S}}|$ and the maximum contraction rate $|\dot{S}|_{max}$ decreased with the stall force (Figs. 2 *C*, and 3 *D* and *E*). Here $|\bar{\dot{S}}| = (S_e - S_c)/\tau_c$. In contrast, the stall force delayed *V. convallaria* in reaching the peak contraction rate, and hence the time of the peak contraction rate τ_{max} increased with the stall force (Fig. 3 *B*). Therefore, the stall force affected the stalk contraction dynamics of *V. convallaria*.

To represent the observed effects of the stall force on contraction dynamics, we found scaling laws of the dynamics parameters using linear fitting based on the method of least squares (Fig. 3). The fitting results suggest the following scaling laws: $\tau_c \sim F_d^{0.40}$, $\tau_{max} \sim F_d^{0.30}$, $|\bar{\dot{S}}| \sim F_d^{-0.53}$ and $|\dot{S}|_{max} \sim F_d^{-0.51}$. Although these parameters showed a dependence on the stall force, their respective ratios did not

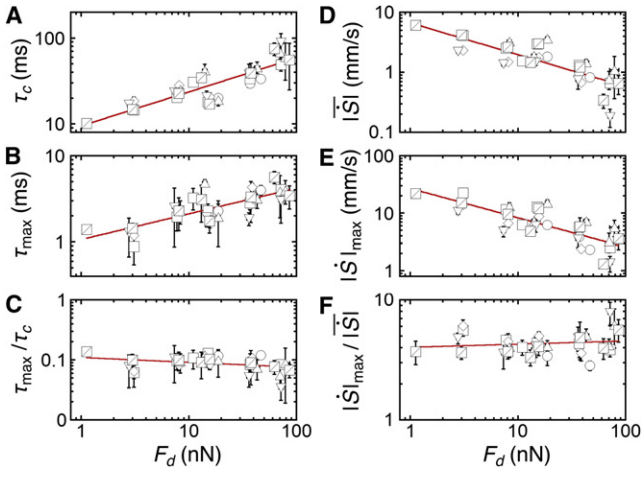

FIGURE 3 Dynamics of stalled contraction of *V. convallaria*. (*A–F*) Contraction time τ_c, time of the maximum contraction rate τ_{max}, ratio of τ_{max} to τ_c, average contraction rate $|\bar{\dot{S}}|$ $(= (S_e - S_c)/\tau_c)$, maximum contraction rate $|\dot{S}|_{max}$, and ratio of $|\dot{S}|_{max}$ to $|\bar{\dot{S}}|$ are shown as functions of the zooid drag force ($n = 6$ cells). Red fitting lines suggest $\tau_c \sim F_d^{0.40}$, $\tau_{max} \sim F_d^{0.30}$, $\tau_{max}/\tau_c \sim F_d^{-0.08}$, $|\bar{\dot{S}}| \sim F_d^{-0.53}$, $|\dot{S}|_{max} \sim F_d^{-0.51}$, and $|\dot{S}|_{max}/|\bar{\dot{S}}| \sim F_d^{0.03}$, respectively. Error bars: SD.

change significantly even with a change by two orders of magnitude in the stall force: $\tau_{max}/\tau_c \sim F_d^{-0.08}$ and $|\dot{S}|_{max}/|\dot{S}| \sim F_d^{0.03}$.

The viscous resistance also influenced the force generation of the spasmoneme. The residual contraction force F_r increased with the stall force (Fig. 4 *A*); that is, the spasmoneme generated higher contractile forces to overcome the increased resistance. Because the residual contraction force increased linearly with respect to the stalk length ratio L_{sc}/L_{se}, the isometric force F_{iso} of *V. convallaria* was estimated to be 150–350 nN by extrapolating the residual contraction force up to $L_{sc}/L_{se} = 1$ (Fig. 4 *B*). The measured values of F_{iso} agree well with previous measurements obtained using centrifugal forces and micropipettes (19).

Stalk-length dependence

It is noticeable in Fig. 4 *A* that the *V. convallaria* cell with the longer stalk generated higher isometric tension than the one with the shorter stalk. Having plotted F_{iso} as a function of L_{se}, we found that longer-stalked *V. convallaria* developed a higher isometric force and the values of the isometric force appeared to increase with a linear dependence on the stalk length (Fig. 4 *B*). This means that the contractile force maximally generated by the unit length of the stalk (or the spasmoneme) was roughly constant. A linear regression between F_{iso} and L_{se} suggests that 1 μm of the *V. convallaria* stalk could generate a contraction force of up to ~2.5 nN ($F_{iso}/L_{se} \sim 2.5$ nN/μm).

The mechanical work done by *V. convallaria* cells shows a similar stalk-length dependency. The work required to overcome the external viscous resistance could be approximated to be $W \approx F_d(S_e - S_c)$. As the stall force increased, the spasmoneme worked more (Fig. 4 *C*). Normalized with the stalk length, the work conformed to a scaling law $W/L_{se} \sim F_d^{0.88}$ with the maximum of ~30 fJ/μm. Because the Ca^{2+} binding energy per 1 μm of the spasmoneme is 176 fJ, W/L_{se} can be converted to the energy conversion efficiency of the spasmoneme, and the maximum efficiency of the spasmoneme is ~17%, which agrees with value achieved in stagnant PVP medium (2). Therefore, the scaling law of W/L_{se} suggests that the spasmoneme converted energy from Ca^{2+} binding to mechanical work with higher efficiency under higher resistance. However, these energetics estimations suggest lower bounds to total work, because neither work for stalk deformation nor additional viscous resistance due to acceleration was considered. The mechanical power that dissipated during the stalled stalk contraction could be similarly approximated to be $P \approx F_d|\dot{S}|_{max}$. The estimated power was on the order of 10–100 pW, but it was one or two orders lower than the maximum power dissipated during the normal contraction (~1 nW) (2).

The linear length dependence of the isometric force is a well-known characteristic of sarcomeres of striated muscles. A striated muscle consists of myofibrils composed of repeating sections of sarcomeres. Whereas the isometric tension of a myofibril depends on its cross-sectional area (22), the isometric tension of a sarcomere depends on its length (23). When the sarcomere is extended beyond its resting length, where the isometric tension is maximal, fewer cross-bridges connecting the thin and thick filaments participate in force generation. Consequently, the isometric tension of the sarcomere linearly decreases with respect to the sarcomere length. This linearity suggests that each active cross-bridge generates a constant magnitude of force.

Based on findings for the sarcomere, we assume that the isometric tension of *V. convallaria* depends on the number and maximum force of motor units in the spasmoneme, which presumably are spasmoneme filaments or spasmin molecules. It is a reasonable assumption that the number density of the motor units is constant along the spasmoneme. Because the spasmoneme diameter (1.4 $\pm$ 0.1 μm) showed negligible deviations compared with the stalk length range (55–135 μm) among *V. convallaria* cells, the total number of motor units will be linearly proportional to the spasmoneme length. Furthermore, if each motor unit maximally generates a certain magnitude of force, the isometric force of *V. convallaria* will linearly depend on the stalk length. This hypothesis is also supported by the coincidence of W/L_{se} shown in Fig. 4 *C*, which suggests that the spasmoneme of the unit length performed a similar amount of mechanical work at a given resistance, and that the mechanical work of the spasmonemal motor units accumulated along the stalk.

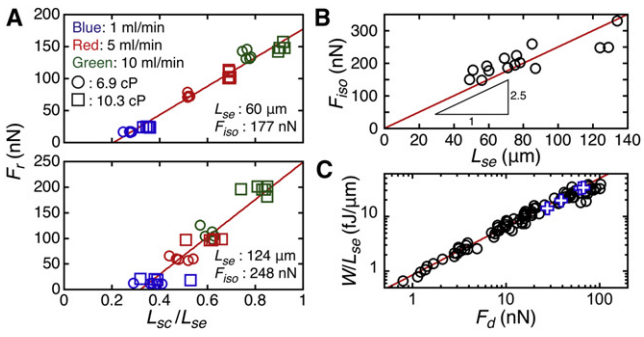

FIGURE 4 Mechanical force and work done by the *V. convallaria* stalk. (*A*) The residual contraction force (F_r) retained by two stalled *V. convallaria* cells as a function of the stalk length ratio (L_{sc}/L_{se}). Each graph shows the length of the relaxed stalk and the estimated isometric force (the red line is the fitting line). (*B*) The isometric tension of *V. convallaria* increased with the stalk length. The regression line passes through the origin because the stalk with zero length cannot generate any contraction force. The red regression line suggests $F_{iso}/L_{se} \sim 2.5$ nN/μm. (*C*) The minimum mechanical work normalized by the stalk length ($n = 15$ cells) shows that *V. convallaria* worked more as the zooid drag force increased. Blue cross: work done by *V. convallaria* in stagnant PVP media (2). The red fitting line suggests a scaling law of $W/L_{se} \sim F_d^{0.88}$.

Force and work per motor unit

Based on our hypothesis, we estimated the force and work of the spasmonemal motor unit. Because the length of the spasmoneme filaments is unknown (24,25), we evaluated the contractile force per 1 μm of the filament. The fibrillar mass accounts for ~85% of the cross-sectional area of the spasmoneme, and the filaments are ~3 nm apart (9,26). Therefore, the spasmoneme has ~2×10^5 filaments in its cross section, and 1 μm of the spasmoneme filament can maximally generate a contractile force of ~10 fN ($\approx$2.5 nN/2×10^5).

We were also able to estimate the maximum force and work per spasmin molecule. Based on the measurement with *Zoothamnium*, we postulated that 1.6×10^{-17} mol (9.5×10^6 atoms) of Ca^{2+} bind to 1 μm of the spasmoneme (2), while approximately two Ca^{2+} atoms bind to one spasmin molecule (27). Thus, it was estimated that 1 μm of the spasmoneme contains ~5×10^6 spasmin molecules and hence one spasmin molecule can generate force of up to ~0.5 fN. Similarly estimated, the maximum work per spasmin molecule is ~6×10^{-21} J, which is 50% higher than the thermal energy ($k_BT = 4 \times 10^{-21}$ J).

DISCUSSION

To carefully measure the isometric tension of live *V. convallaria*, we applied viscous drag to *V. convallaria* using the microfluidic technique. The applied resistance stalled stalk contraction of *V. convallaria*, and the spasmoneme generated higher contractile forces. Previous studies also imposed viscous drag on contracting *V. convallaria* by placing the cell in stagnant, highly viscous media (2,15). Although the drag hindered stalk contraction in both cases, there are noticeable differences between our study and the previous ones. First, *V. convallaria* could fully contract in the stagnant fluid but not in the channel flow. Second, τ_{max} depended on the amount of drag in our study, whereas it did not in the previous studies. Third, the time courses of L_s were well represented by $[\mathrm{sech}(t/c_1)^{c_2}]^{c_3}$ (c_1, c_2 and c_3 : fitting constants) in the previous study (2), whereas those of S were not in our study. Although L_s is a function of S and R (or R_z), S is expected to well represent L_s because the change in R is negligible compared with that in S. These differences seem to be due to a difference in resistance type. In the stagnant fluid, *V. convallaria* experiences temporary resistance only when it contracts, and there is negligible drag on the zooid at the beginning and ending of stalk contraction. In contrast, the cell is always under consistent viscous drag in the channel flow regardless of its motion, and its contraction mechanism operates under the influence of the stall force. Therefore, types of applied stall force seem to have affected the stalk contraction behavior of *V. convallaria*.

One noticeable energetics aspect of *V. convallaria* is that its stalk contraction is power-limited (2,15). When *V. convallaria* contracts in stagnant fluids of various viscosities, its maximum power changes negligibly compared with changes in viscosity and thus applied drag. Based on power-limitedness, a scaling law $|\dot{L}_s|_{max} \sim F_{d,max}^{-1}$ was suggested. In contrast, it was observed in this study that $|\dot{S}|_{max} \sim F_d^{-0.51}$ (Fig. 3 *E*). This does not necessarily mean that power-limitedness is not valid for stalk contractions in the channel flow, because the observed scaling law was empirical rather than derived from the maximum power dissipation characteristics. One must determine the time course of drag on the zooid to estimate the maximum power dissipated by the spasmoneme. In addition to drag from the channel flow (F_d), the moving zooid experienced more drag due to its own motion (see Supporting Material). However, this additional component was difficult to estimate because the distance between the zooid and the channel surface could not be measured. Although the maximum power dissipation was not estimated and the power-limitedness was not confirmed, the observed scaling law of $|\dot{S}|_{max}$ serves as a reference for the dynamics of stalled stalk contraction, along with the scaling laws suggested in Fig. 3.

The isometric tension of the stalk was measured to characterize the maximal force of contracting *V. convallaria*. We normalized the measured isometric tension with the stalk length based on their approximate linear relation (Fig. 4 *B*). This normalization requires an assumption that the tension per unit length of the spasmoneme is constant along the spasmoneme. However, it is not known whether the spasmoneme has lengthwise variations in its contractility. Instead, any differences in local contractility can be inferred based on differences in threshold levels for contraction along the stalk. In previous studies, mechanical, electrical, and chemical stimuli were applied locally to the stalk of *Vorticella* or *Carchesium*. The threshold levels of those stimuli were higher for the upper part of the stalk (near the zooid) than those for the lower part (near the rootlet) (28–30). This difference might come from lengthwise differences in the Ca^{2+} binding affinity of the spasmoneme (29) or the sheath thickness (30). In contrast, it was previously reported for *Carchesium* that electric stimulation of a constant threshold induced contraction regardless of stimulated points on the stalk (31), and that there was no difference in the threshold of Ca^{2+} concentration among fragments of spasmoneme and the intact spasmoneme (32). Therefore, it requires more study to determine whether contractility is uniform along the spasmoneme, and glycerinated stalks can be employed to confirm the lengthwise uniform contractility and stalk-length dependence of isometric tension. Although our assumption needs to be verified, F_{iso}/L_{se} can serve as a representative parameter to characterize the maximum contractile force of the *Vorticella* stalk.

It is meaningful to compare the force and work of the spasmoneme with those of similar biological or engineering systems. In terms of the isometric tensile stress, the

spasmoneme (10–23 g/mm^2) is comparable to muscle (10–36 g/mm^2) (33) and outperforms the forisome (~1 g/mm^2), an ATP-independent Ca^{2+}-powered protein body in the sieve system of leguminous plants (34). The work density of the spasmoneme (~20 kJ/m^3) is also less than or comparable to that of muscle (~40 kJ/m^3) and polymer actuators (10–300 kJ/m^3) (33). Hence, the spasmoneme still has potential as a model system for biomimetic actuators. Compared with other motor proteins, however, the force of a spasmin molecule seems to be underestimated due to lack of information about the spasmin of the *V. convallaria* spasmoneme. Based on various single-molecule biophysical measurements, it is known that a single molecule of dynein, kinesin, and myosin can generate force of 3–7 pN (35), which is four orders higher than our estimate for spasmin. A reason for this uncertainty is that the number of spasmin molecules in the *V. convallaria* spasmoneme was estimated based on the amount of Ca^{2+} bound to the *Zoothamnium* spasmoneme. Although both *Vorticella* and *Zoothamnium* show Ca^{2+}-driven contractions, their detailed contraction mechanism and Ca^{2+}-binding characteristics can be different (36). Another reason is that spasmin may not be the motor protein of the spasmoneme even though it is the major component of the spasmoneme. It was previously suggested that spasmin may regulate its binding partner, spaconnectin, upon Ca^{2+} binding, and that spaconnectin may be responsible for contraction of the spasmoneme (11,37,38). Therefore, more information on the biophysical mechanism of the spasmoneme contraction is required to estimate force and work per motor unit of the spasmoneme based on our experimental measurement.

It also must be pointed out that our estimates rely on the main assumption that the force of motor units within the spasmoneme accumulates not only in parallel but also in series. Because it may seem counterintuitive for forces to accumulate in series, we suggest such a conceptual spring model for the spasmoneme (Fig. 5). The model consists of two parallel deformable rods and a series of uniformly spaced N Hookean springs. Connecting the two rods, each spring is oriented parallel to the rods. Upon contraction, the spring constant of the springs increases from k_e to k_c, which leads the model to shorten from L_e to L_c. When forces are applied to stretch the contracted model to L_e, the applied force corresponds to the isometric tension of the model. Because each spring exerts force of $k_c(l_e - l_c)$ to the rod, the force is $F_{iso} = Nk_c(l_e - l_c)$. Because L_e is proportional to Nl_e, the isometric force per unit length of the model has a constant value: $F_{iso}/L_e \sim k_c(1 - l_c/l_e)$. Therefore, there is a similarity between the spasmoneme of *V. convallaria* and the spring model in that the isometric tension is proportional to the length of the motor. Although the conceptual spring model gives a rudimentary insight into how motor units can be arranged in the spasmoneme, the three-dimensional structure of the spasmoneme must be identified to verify our hypothesis and estimation.

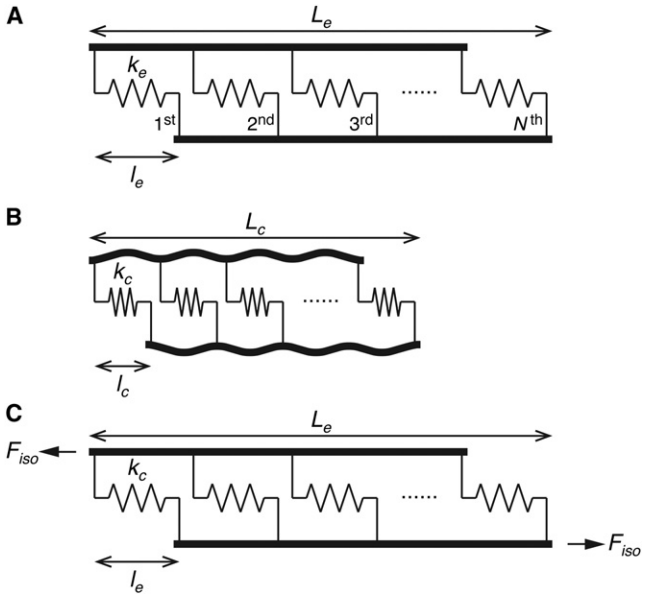

FIGURE 5 Conceptual spring model for the spasmoneme of *V. convallaria*. The model consists of two parallel deformable rods and N Hookean springs connecting the rods. (*A*) Relaxed state. The spring constant and length of the springs are k_e and l_e, respectively. The length of the model L_e is proportional to Nl_e. (*B*) Contracted state. Because the spring constant has increased to k_c, the springs contract to l_c, leading the model to shorten to L_c. (*C*) Isometric state. A force of $F_{iso} = Nk_c(l_e - l_c)$ is required to stretch the model to L_e, and hence the force is proportional to the model length, $F_{iso} \sim k_c(1 - l_c/l_e)L_e$.

The spasmoneme of *V. convallaria* was previously regarded as a stalked muscle or a primitive type of muscle because of its ability to contract, and early studies tried to connect the spasmoneme to muscle (12). Later, it was revealed that the contraction machinery of the spasmoneme is different from that of muscle because the spasmoneme contraction is powered not by ATP but by calcium (5), and because the volume and birefringence of the spasmoneme change significantly before and after contraction (12,17). In addition, the spasmoneme's motor protein is not myosin, because actin is absent in the spasmoneme (7). Instead, the contraction of the spasmoneme is relevant to motility phenomena based on centrin, a 20 kDa EF-hand Ca^{2+}-binding protein that is ubiquitously found in microtubule organizing centers of eukaryotic cells, since spasmin is a homolog of centrin (7,8). However, the contraction mechanism of the spasmoneme is still unknown. Several models have been suggested and discussed to date (1,39), including an electrostatic model (5) and an entropic rubber model (17,38). The electrostatic model is thought to be the least probable because it cannot account for the Ca^{2+} specificity of the spasmoneme. The entropic rubber model seems inconsistent with our observation because when it is applied to the glycerinated spasmoneme of *Zoothamnium*, the model suggests that the isometric tension may be determined the fractional extension of the spasmoneme rather

than by the spasmoneme length (38). Among suggested models, it is most probable that the nanofilaments of the spasmoneme consist of molecules of spasmin and spaconnectin, and that folding of the filaments induced by Ca^{2+} binding causes the spasmoneme to contract (11,38). A similar model was suggested for centrin-based contraction (10). However, it remains to be determined whether the nanofilaments are composed of the two proteins and whether they fold upon Ca^{2+} binding. Furthermore, it will be possible to judge whether the folding filament model is compatible with our observations once it is revealed how the filaments are organized in the spasmoneme.

V. convallaria is a model microorganism for Ca^{2+}-based cell motility and bioinspired actuators because its spasmoneme generates forces on the order of 10–100 nN, converting energy from Ca^{2+} binding. By applying consistent viscous drag, we investigated the dynamics of stalled stalk contraction of *V. convallaria* and measured its isometric tension. Our measurements show that longer-stalked *V. convallaria* cells developed higher isometric tension and that the maximal force and work of *V. convallaria* linearly depended on the stalk length. On the basis of these observations, we suggest that the motor units of the spasmoneme may be organized in such a way that the force and work of each unit accumulate across the cross section and along the length of the spasmoneme.

SUPPORTING MATERIAL

Seven figures, two tables, and references (40–45) are available at http://www.biophysj.org/biophysj/supplemental/S0006-3495(12)00851-X.

We thank the reviewers for their constructive comments, and S.R. thanks Dr. Hiroshi Asai for discussion about the isometric tension of glycerinated *V. convallaria*.

This study was supported by the Institute for Collaborative Biotechnologies through grant DAAD19-03-D-0004 to P.M. from the U.S. Army Research Office. Initial experiments were supported by a grant from Dupont to P.M.

REFERENCES

1. Mahadevan, L., and P. Matsudaira. 2000. Motility powered by supramolecular springs and ratchets. *Science.* 288:95–100.
2. Ryu, S., and P. Matsudaira. 2010. Unsteady motion, finite Reynolds numbers, and wall effect on *Vorticella convallaria* contribute contraction force greater than the Stokes drag. *Biophys. J.* 98:2574–2581.
3. McMahon, T. A., and J. T. Bonner. 1983. On Size and Life. Scientific American Library, New York.
4. Moriyama, Y., S. Hiyama, and H. Asai. 1998. High-speed video cinematographic demonstration of stalk and zooid contraction of *Vorticella convallaria*. *Biophys. J.* 74:487–491.
5. Hoffmann-Berling, H. 1958. [The mechanism of a new contraction cycle differing from muscle contraction]. *Biochim. Biophys. Acta.* 27:247–255.
6. Amos, W. B. 1971. Reversible mechanochemical cycle in the contraction of *Vorticella*. *Nature.* 229:127–128.
7. Amos, W. B., L. M. Routledge, and F. F. Yew. 1975. Calcium-binding proteins in a vorticellid contractile organelle. *J. Cell Sci.* 19:203–213.
8. Salisbury, J. L. 1995. Centrin, centrosomes, and mitotic spindle poles. *Curr. Opin. Cell Biol.* 7:39–45.
9. Amos, W. B. 1972. Structure and coiling of the stalk in the peritrich ciliates *Vorticella* and *Carchesium*. *J. Cell Sci.* 10:95–122.
10. Salisbury, J. L. 2004. Centrosomes: Sfi1p and centrin unravel a structural riddle. *Curr. Biol.* 14:R27–R29.
11. Asai, H. 2005. Ca^{2+}-driven contraction of spasmoneme in Vorticellidae. *Jpn. J. Protozool.* 38:133–152.
12. Sugi, H. 1961. Volume change during contraction in the stalk muscle of *Carchesium*. *J. Fac. Sci. Univ. Tokyo Section IV: Zoology.* 9:155–170.
13. Knoblauch, M., and W. S. Peters. 2004. Biomimetic actuators: where technology and cell biology merge. *Cell. Mol. Life Sci.* 61:2497–2509.
14. Marden, J. H., and L. R. Allen. 2002. Molecules, muscles, and machines: universal performance characteristics of motors. *Proc. Natl. Acad. Sci. USA.* 99:4161–4166.
15. Upadhyaya, A., M. Baraban, …, L. Mahadevan. 2008. Power-limited contraction dynamics of *Vorticella convallaria*: an ultrafast biological spring. *Biophys. J.* 94:265–272.
16. Moriyama, Y., K. Yasuda, …, H. Asai. 1996. Ca(2+)-induced tension development in the stalks of glycerinated *Vorticella convallaria*. *Cell Motil. Cytoskeleton.* 34:271–278.
17. Weis-Fogh, T., and W. B. Amos. 1972. Evidence for a new mechanism of cell motility. *Nature.* 236:301–304.
18. Rahat, M., Y. Pri-Paz, and I. Parnas. 1973. Properties of stalk-'muscle' contractions of *Carchesium* sp. *J. Exp. Biol.* 58:463–471.
19. France, D. C. 2007. Structure and mechanics of the spasmoneme, a biological spring within the protozoan *Vorticella convallaria*. Ph.D. thesis, Massachusetts Institute of Technology, Cambridge, MA.
20. Vacchiano, E. J., J. L. Kut, …, H. E. Bushe. 1991. A novel method for mass-culturing *Vorticella*. *J. Protozool.* 38:608–613.
21. Pozrikidis, C. 2000. Effect of pressure gradient on viscous shear flow past an axisymmetric depression or protuberance on a plane wall. *Comput. Fluids.* 29:61–637.
22. Sugi, H. 1992. Molecular mechanism of actin-myosin interaction in muscle contraction. *In* Advances in Comparative and Environmental Physiology. Muscle Contraction and Cell Motility: Molecular and Cellular Aspects, *Vol. 12*. H. Sugi, editor. Springer-Verlag, Berlin. 132–171.
23. Gordon, A. M., A. F. Huxley, and F. J. Julian. 1966. The variation in isometric tension with sarcomere length in vertebrate muscle fibres. *J. Physiol.* 184:170–192.
24. Sotelo, J. R., and O. Trujillo-Cenoz. 1959. The fine structure of an elementary contractile system. *J. Biophys. Biochem. Cytol.* 6:126–128.
25. Allen, R. D. 1973. Contractility and its control in peritrich ciliates. *J. Protozool.* 20:25–36.
26. Konior, K., S. McCutcheon, and H. E. Bushe. 2009. Subcellular centrin localization within distinct compartments of *Vorticella convallaria*. *Trans. Ill. Acad. Sci.* 102:161–174.
27. Routledge, L. M., W. B. Amos, …, T. Weis-Fogh. 1975. Microprobe measurements of calcium binding in the contractile spasmoneme of a vorticellid. *J. Cell Sci.* 19:195–201.
28. Ueda, K. 1952. Studies on the stalk muscle of *Carchesium* (I). *Zool. Mag.* 61:367–371.
29. Ochiai, T., H. Asai, and K. Fukui. 1979. Hysteresis of contraction-extension cycle of glycerinated *Vorticella*. *J. Protozool.* 26:420–425.
30. Katoh, K., and Y. Naitoh. 1992. A mechanosensory mechanism for evoking cellular contraction in *Vorticella*. *J. Exp. Biol.* 168:253–267.
31. Sugi, H. 1960. Propagation of contraction in the stalk muscle of *Carchesium*. *J. Fac. Sci. Univ. Tokyo Section IV: Zoology.* 8:603–615.
32. Hawkes, R. B., and M. Rahat. 1976. Contraction and volume reduction of the glycerolated *Carchesium* spasmoneme: effects of alkali earth cations. *Experientia.* 32:160–162.

33. Madden, J. D. W., N. A. Vandesteeg, …, I. W. Hunter. 2004. Artificial muscle technology: physical principles and naval prospects. *IEEE J. Oceanic Eng.* 29:706–728.

34. Knoblauch, M., G. A. Noll, …, W. S. Peters. 2003. ATP-independent contractile proteins from plants. *Nat. Mater.* 2:600–603.

35. Shingyoji, C., H. Higuchi, …, T. Yanagida. 1998. Dynein arms are oscillating force generators. *Nature.* 393:711–714.

36. Itabashi, T., K. Mikami, and H. Asai. 2003. Characterization of the *spasmin 1* gene in *Zoothamnium arbuscula* strain Kawagoe (protozoa, ciliophora) and its relation to other spasmins and centrins. *Res. Microbiol.* 154:361–367.

37. Asai, H., T. Ninomiya, …, Y. Moriyama. 1998. Spasmin and a putative spasmin binding protein(s) isolated from solubilized spasmonemes. *J. Eukaryot. Microbiol.* 45:33–39.

38. Moriyama, Y., H. Okamoto, and H. Asai. 1999. Rubber-like elasticity and volume changes in the isolated spasmoneme of giant Zoothamnium sp. under Ca^{2+}-induced contraction. *Biophys. J.* 76:993–1000.

39. Routledge, L. M., W. B. Amos, …, T. Weis-Fogh. 1976. New calcium-binding contractile proteins. *In* Cell Motility. R. Goldman, T. Pollard, and J. Rosenbaum, editors. Cold Spring Harbor Laboratory Press, Cold Spring Harbor, NY. 93–113.

40. White, F. M. 1991. Viscous Fluid Flow. McGraw-Hill, New York.

41. Pasol, L., A. Sellier, and F. Feuillebois. 2006. A sphere in a second degree polynomial creeping flow parallel to a wall. *Q. J. Mech. Appl. Math.* 59:587–614.

42. Chaoui, M., and F. Feuillebois. 2003. Creeping flow around a sphere in a shear flow close to a wall. *Q. J. Mech. Appl. Math.* 56:381–410.

43. Staben, M. E., A. Z. Zinchenko, and R. H. Davis. 2003. Motion of a particle between two parallel plane walls in low-Reynolds-number Poiseuille flow. *Phys. Fluids.* 15:1711–1733.

44. Zeng, L., F. Najjar, and S. Balachandar. 2009. Forces on a finite-sized particle located close to a wall in a linear shear flow. *Phys. Fluids.* 21:033302.

45. Sugihara-Seki, M., and R. Skalak. 1997. Force acting on spheres adhered to a vessel wall. *Biorheology.* 34:249–260.

46. Brooks, S. B., and A. Tozeren. 1996. Flow past an array of cells that are adherent to the bottom plate of a flow channel. *Comput. Fluids.* 25:741–757.